STREAM

IST-1999-10341

STREAM CONSORTIUM:
CNR-LAMEL / ST Microelectronics / ISEN / SOFT IMAGING SYSTEM / University of Sheffield / IMEC / CNR-IESS / University of Perugia

DELIVERABLE D2

Workpackage WP3

Lead participant: CNR-LAMEL

Assessment of the TEM/CBED procedure for strain determination in <130> zone axis

Main Author	A.Armigliato, CNR-LAMEL		
Contributing authors	R.Balboni, S.Frabboni, CNR-LAMEL		
Date:	29- 02 - 2000	***Doc.No:***	IST10341-LA-RP001
Keywords:	Strain, isolation structures, electron microscopy, convergent beam electron diffraction		

Distribution list	**Project Officer:** M.Korn (3 copies) **All Partners:** P. Colpani ST Microelectronics V. Senez ISEN T. Schilling Soft Imaging System A.G.Cullis USFD (University of Sheffield) I. De Wolf IMEC S. Lagomarsino CNR-IESS G. Carlotti UniPg (University of Perugia)

Table of contents

1. Introduction

The project STREAM deals with one of the major issues of concern for the future deep-submicron IC technologies regarding yield, device performance and stability and product reliability, namely the mechanical stress built up in the layers and substrate. It is therefore important to give a quantitative account of these stresses and this can only be achieved by disposing of reliable, performant (resolution) and quantitative techniques for the local stress determination in the substrate, of adequate and dedicated process simulation tools and of sensitive methods to analyse the stress effects on device performance.

The evolution of the integrated circuits is determined by the need of a steady increase in the ability to handle the information, and this is reflected from the technological viewpoint in the need of a higher and higher miniaturisation of the various components of the IC.

In Table 1 are reported the most relevant parameters of the ICs for the last few years, together with a forecast for the upcoming years.

Table 1 Evolution of integrated circuit (IC) technology during the last few years and a forecast of the years 2001-2004. DRAM: Dynamic Random Access Memories; MPU: Microprocessors. Technology node: Development of the Technological generation.

	1997[1]	1999[2]	2001	2002	2003	2004
Technology node (from NTRS[3] 1994)	-	-	*180 nm*	-	-	*130 nm*
Technology node (from ITRS 1997)	*250 nm*	*180 nm*	-	*150 nm*	*130 nm*	-
Technology node (from ITRS 1999)	-	*180 nm*	-	*130 nm*	-	-
DRAM ½ pitch (nm)	*250*	*180*	*150*	*130*	*120*	*110*
MPU Gate Length (nm)	*200*	*140*	*100*	*85*	*80*	*70*
Memory (DRAM)						
DRAM cell size (μm^2)	*0,56*	*0,26*	*0,18*	*0,10*	*0,08*	*0,065*
FLASH cell size (NOR, μm^2)	*0,6*	*0,34*	*0,24*	*0,17*	*0,15*	*0,13*
Chip size at introduction (mm^2)	*280*	*400*	*438*	-	*480*	-
Number of mask levels	-	*20*	*20*	*21*	*21*	*21*
Interconnect levels	*6*	*6-7*	*7*	*7-8*	*8*	*8*
Faults per Mask Level	-	*141*	*129*	*117*	*112*	*107*

With the scaling down of the IC size, the problem of the mechanical stresses induced by the fabrication process into the active area of a device becomes of increasing importance. To determine the stress/strain field distribution in deep sub-micron devices an experimental technique with a high spatial resolution and good sensitivity is required. The most suitable technique presently available is the convergent beam electron diffraction technique of the transmission electron microscopy (TEM/CBED).

The main scope of the project STREAM is to develop an experimental methodology based on the TEM/CBED technique to measure lattice strain in silicon with a spatial resolution down to 1 nm. The strain tensor will be determined by this technique on structures fabricated on 8” silicon

[1] From International Technology Roadmap for Semiconductors (IRST):1997
[2] From ITRS 1999
[3] National Technology Roadmap for Semiconductors

wafers, which will comprise CMOS devices with a linewidth down to 0.15 μm for non volatile memories (NVM).

In this report it will be described the principles of TEM/CBED and the procedure to deduce the strain tensor in a sub-micrometric region of a sample from the experimental measurements. A recent application to the investigation of strain field distribution in local isolation structures (LOCOS) will be detailed.

2. Principles and practice of CBED

2.1 Characteristics of a modern transmission electron microscope (TEM).

The use of transmission electron microscopy for diffraction experiments benefits from the strong interaction of electrons with matter. Due to the large elastic cross section, the volume of material needed for electron diffraction is 10^5-10^9 smaller than that of X-rays. So useful patterns can be obtained in cross sections of microelectronic devices, few hundreds of nm thick, as in the case of the CBED applications.

The illumination system of a modern TEM electron source includes an electron source and a number of condenser lenses. Two main electron sources are available: the lanthanum hexaboride (LaB_6) single crystal and the field emission gun (FEG). We will consider here only the thermal (or Schottky type) FEG, which consists of a zirconiated W filament and is presently of more widespread use than the cold FEG.

The source brightness *B*, defined as the current density per unit solid angle ($A/cm^2/sr$), determines the total current that can be focused on a specimen, which is the key parameter for the use of very small probes in CBED experiments. As *B* depends on the acceleration voltage *V*, it is convenient to work with the so called reduced brightness $B_r=B/V$. The theoretical maximum electron intensity I_{th} is related to the brightness *B* through the equation:

$$I_{th} = B_r(p a^2 d^2 / 4)$$

where α is the semiangle of the probe-forming lens and *d* the diameter of the source. From Table 2 it can be seen how the electron energy spread is mainly affected by the temperature of the tip.

Table 2 Characteristics of the most common electron sources

Electron source	Tip temperature (K)	Reduced Brightness (A/cm^2srV)	Source size (nm)	Energy spread (eV)
LaB_6	2100	10-100	1000	0.4-1.5
Schottky FEG	1800	10^3-10^4	20	0.3-1.5

The condenser system consists of several lenses, to allow very flexible illumination, from a parallel beam to a very small and intense beam for CBED analysis (and in general for spot analysis). Typical minimum spot diameters are 2 nm for LaB_6 filaments and 0.5 nm for FEG electron guns. In practice, the spot employed for the CBED work performed so far at CNR-LAMEL was about 10 nm in diameter.

The standard size of a TEM specimen is a thin disk with a diameter of 3 mm. The sample holder must allow the specimen to be tilted in any orientation, which requires tilting about two mutually perpendicular axes (or a combination of specimen tilt and rotation). Moreover, to enhance the visibility of the features present in the CBED pattern (see §2.2) it is advisable to cool the sample. Commercial holders coolable by liquid nitrogen to a temperature of about 100 K are available and have been used in the TEMs of the partners of STREAM (CNR-LAMEL, ST and

USFD). An added advantage of the cooling holders is the reduction of specimen contamination, which can be a problem when working with small and intense electron probes.

As to the systems for recording of the diffraction patterns and of the images of the microelectronic device, the traditional photographic film has been practically superseded by slow-scan CCD cameras. In fact, the major disadvantages of films are the required processing steps in a darkroom, the very limited linearity of the recorded intensity and the need for a digitisation if the images are to be processed by a computer (which is the case for the CBED patterns, see Sect.4).

Slow-scan CCD cameras consist of a scintillator to transform electrons into light, which is coupled through a fibre-optics device to a high quality CCD detector; moreover, to reduce noise, the CCD camera is generally cooled down to about –20 C. The size of the chip is in general of 1" and it consists of an array of 1024X1024 pixels; its linearity is very high, as the dynamic range is 2^{12} to 2^{16}:1 (to be compared with the 200:1 range of a photographic film). In addition, the pattern is immediately available in digital form, so the TEM parameters can be adjusted if needed in real time; the intensity required for a good CBED pattern is much lower than for a film, so smaller spots can be used, which results in a higher spatial resolution.

Slow-scan CCD of a commercial type are available for the STREAM project in the TEM labs of the three above mentioned partners. The digital CBED patterns so obtained will be used for the development of the automatic procedure for the determination of strain tensor by the partner Soft Imaging System (SIS)

In some microscopes it is also available an electron spectrometer which can (i)analyse the energy spectrum of the transmitted electrons, which can be used as a microanalytical technique (EELS: Electron Energy Loss Spectrometry) or (ii), more important for CBED, transmits only electrons which are either elastically scattered ('zero loss') or have lost a given energy (e.g. plasmon or characteristic losses) thus forming 'energy filtered' images and diffraction patterns (EFTEM: Energy Filtered Transmission Electron Microscopy). The spectrometers can be inserted after the objective lens ('in column') or below the final screen ('post column').

The possibility of filtering the CBED patterns, i.e. to form them with elastically scattered electrons only, will improve the pattern quality and in turn ease the computer simulation of the details contained therein; the increase in the peak/background ratio is due to the suppression of the plasmon and of a large part of the thermal diffuse scattering. It can be expected that CBED patterns taken at room temperature will be of adequate quality for strain analysis.

In Table 3 are reported the main parameters of the three TEMs that will be used during the STREAM activity

Table 3 Characteristics of the TEMs employed in the project (Fig.2.1.1), useful for CBED experiments.

Microscope	*Partner*	*Electron source*	*Max.Voltage (kV)*	*Min. spot size for CBED (nm)*	*Energy filter*	*Slow-scan CCD camera*
Philips CM30	CNR-LAMEL	LaB_6	300	10	Not available	Size:1" 1024X1024
LEO 922	ST Microel.	LaB_6	200	5	In column	Size:1" 1024X1024
Jeol 2010F	USFD	Schottky FEG	200	1	Post column	Size:1" 1024X1024

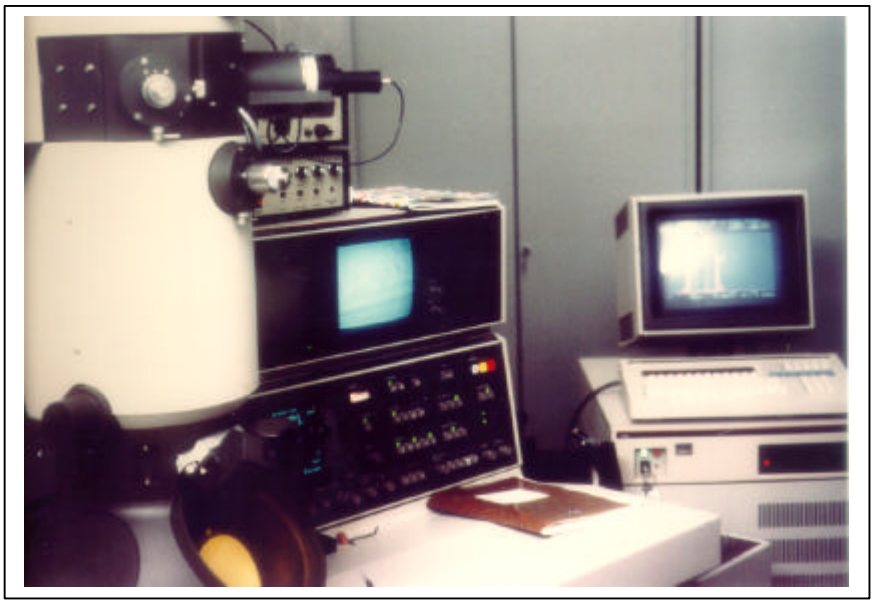

Figure 2.1.1. (left). The Philips CM30 available at the CNR-LAMEL Institute

The LEO 922 TEM installed at the ST Microelectronics Labs.

The Jeol 2010F TEM of the University of Sheffield (USFD)

Finally, some details will be given here on the problem of specimen preparation. To obtain suitable cross sections of the device under investigation, a well established procedure is used. It includes cutting rectangles about 8X10 mm2 from the wafers, then gluing face to face and adding scrap silicon on the back faces, so to obtain a sandwich about 5 mm thick.. Afterwards, these parallelepiped are cut by a diamond saw into 450 micron thick slabs, on which 3 mm disks are indented by ultrasonic drilling for a depth of 20 micron. This step is followed by mechanical polishing on both faces down to less than 20 microns. The resulting disks are finally thinned by ion beam milling to perforation. A careful preparation work gives rise to a cross section, which is transparent to the TEM electron beam in the region of interest.

Alternatively, the mechanical polishing can be replaced by mechanical dimpling of the 100 micron thick disks, resulting in a dish-like sample which is about 5 micron thick at its centre.

All the equipment requested for this procedure (saw, ultrasonic driller, lapping machines, dimpler and ion beam miller) are available in the three TEM laboratories.

2.2 Convergent vs parallel electron beam diffraction

As reported in §2.1, it is possible with the modern TEMs to focus on the specimen an electron beam whose minimum diameter is about 10 nm for thermoionic guns and 1 nm in case of field emission guns. This exceptionally high spatial resolution cannot presently be obtained by other techniques and explains why TEM/CBED plays a dominant role in STREAM, whose main objective is the strain determination in deep submicron CMOS devices.

The second advantage of TEM/CBED, as it will be shown in the following, is that convergent beam diffraction yields a tridimensional information on the crystal lattice of the specimen, thus allowing one to obtain the strain tensor in the analysed region from a single TEM/CBED pattern.

When a parallel electron beam impinges onto a crystalline specimen, a diffraction pattern is formed in the back focal plane of the TEM objective lens. It has the familiar aspect of a spot pattern (Fig.2.2.1a).

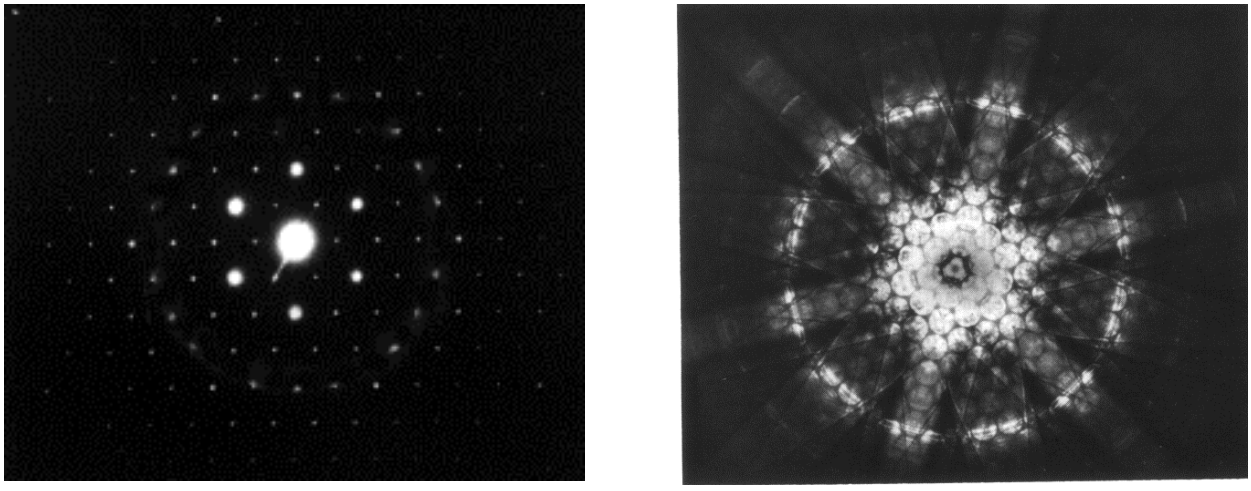

Figure 2.2.1. Typical electron diffraction patterns. a) parallel electron beam; b) convergent beam.

If, instead, the electron beam is focused in the sample plane (convergent beam), the diffraction pattern consists of disks, whose diameter in the back focal plane is related to the beam semi-convergence angle α_i and to the objective focal length f_0 through the relationships:

$$D = 2a_i f_0$$

A ray diagram showing the formation of the disks in the pattern is reported in Fig.2.2.2, whereas an example of a CBED pattern is shown in Fig.2.2.1b.

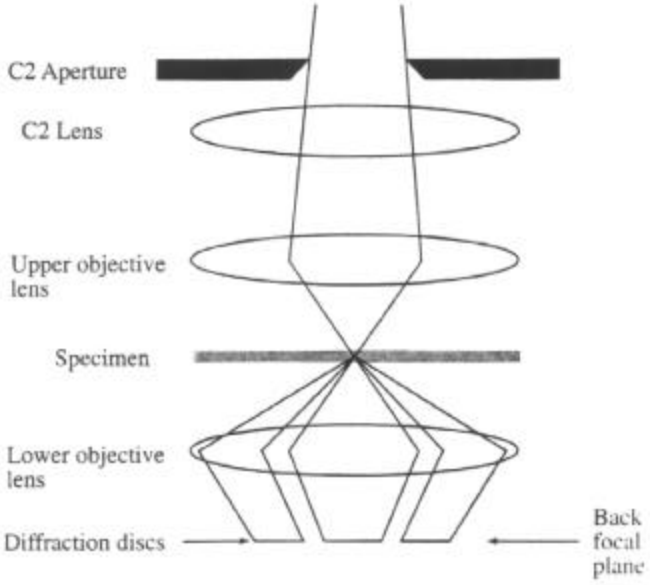

Figure 2.2.2
Ray diagram showing the electron paths in a CBED geometry.
The semi-convergence angle is mainly related to to the second condenser excitation and aperture size (typical values: tenths of a degree)[1]

A close inspection of Fig.2.2.1b reveals the presence of fine dark lines inside the diffracted disks. (Fig.2.2.3). The study of the details of these lines in the central disk of the CBED pattern is the basis of the strain investigation in crystals, as it will be demonstrated below.

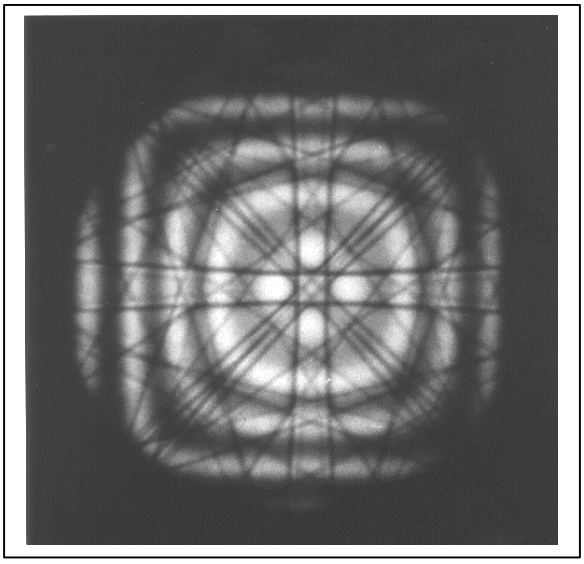

Figure 2.2.3. CBED pattern taken at 100 kV in a <100> zone axis. In this enlarged view, only the central disk is visible. The dark sharp lines are the so-called HOLZ deficit lines[2] and are the basis of the strain analysis method (see text for details). The broad contours arranged in a set of concentric squares are thickness fringes; their spacing decreases by increasing the local sample thickness.

To understand the formation of the dark lines it is necessary to remember that the condition of diffraction for a set of crystal planes (Bragg condition) is given by the intersection of the corresponding point in the reciprocal lattice with the Ewald sphere (Fig.2.2.4)

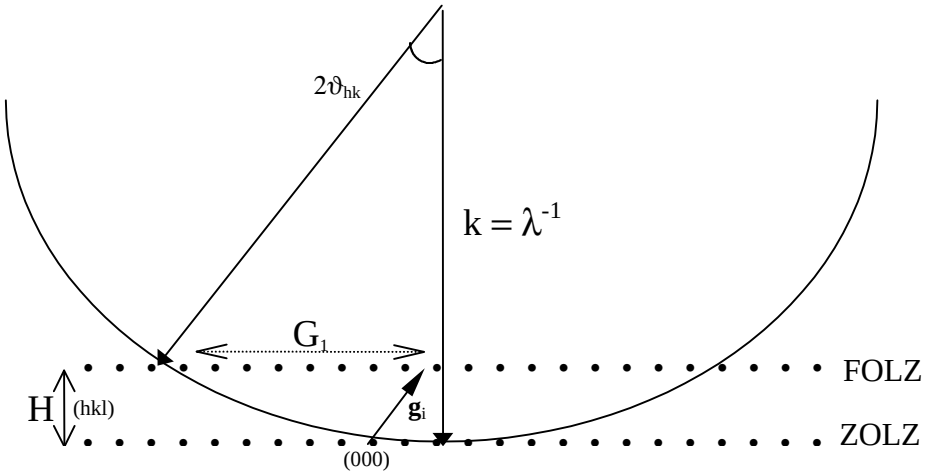

2.2.1 Figure 2.2.4

Graphical representation of the diffraction by means of the Ewald sphere in the reciprocal lattice. The sphere describes the incident beam, whereas the reciprocal lattice describes the crystal lattice of the sample. H is the distance between the Laue zones (nm^{-1}), G_1 is the radius of the FOLZ ring (see Fig.2.2.5), **g** is a diffraction vector of the FOLZ, **k** is the wave vector of the incident beam[3].

As the wavelength of the TEM electrons is very short (λ=0.0037 nm at 100 kV), the radius of the Ewald sphere, given by $|\mathbf{k}|=1/\lambda$, will be much larger than the spot spacing ($|\mathbf{k}|=1/\lambda=270\ nm^{-1}$, whereas, e.g. $\mathbf{g}(220)_{Si}=1.8\ nm^{-1}$). Therefore a large number of reciprocal lattice spots in the ZOLZ (Zero Order Laue Zone) will be intersected. This is the zone represented in a diffraction pattern obtained with a parallel beam, as in Fig. 2.2.1a; the diffracting planes being almost parallel to the incident beam, only a bidimensional information on the crystal lattice can be obtained.

However, when the scattering angle is increased, the intersection between the Ewald sphere and the ZOLZ decreases and eventually ceases (and the diffracted intensity vanishes); for larger angles the sphere intersects the points of the upper FOLZ (First Order Laue Zone), which gives rise to a new series of spots in the pattern, arranged in a ring around the ZOLZ ones. This explains the geometry of a CBED pattern, taken at low magnification, as reported in Fig.2.2.5.

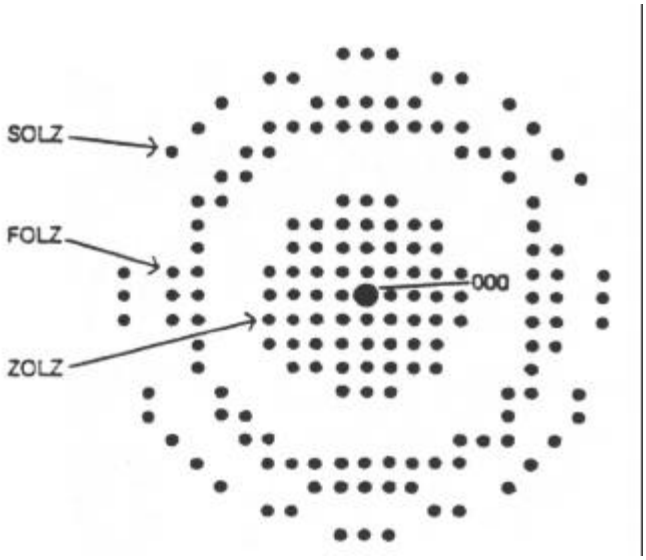

2.2.2 Figure 2.2.5

<100> low magnification CBED pattern, which reproduces the projection on a plane perpendicular to the direction of the incident beam of the Ewald sphere-reciprocal lattice intersection (SOLZ=Second Order Laue Zone).[3]

If the beam convergence is further increased, rings of spots due to higher Laue zones (generally called HOLZ) will appear.

What is important to note is that the reciprocal lattice points in the HOLZ, unlike the ZOLZ ones, have a component also along the axis parallel to the incident beam. This implies that the CBED diffraction patterns give a full tridimensional information on the crystal lattice.

It is known that the Bragg condition is satisfied only at the surface of the Ewald sphere. This implies that in a diffracted disk it will appear a bright line, located at the exact intersection of the reciprocal lattice disk with the surface of the sphere. Due to the aforementioned flatness of the Ewald sphere, these lines are approximately straight lines. They are generally called HOLZ lines, as are due to the excitation of reflections belonging to HOLZ planes. They should not be confused with the more popular Kikuchi lines, as these latter originate from an inelastic scattering and occur also with parallel beams, whereas HOLZ lines, occurring inside a Bragg diffracted disk, are elastically generated and are visible only with convergent beams. However, similarly to Kikuchi lines, HOLZ lines occur in pairs: to the bright line in a diffracted disk (excess line) corresponds a dark line (deficit line) in the central disk of the CBED pattern. This is due to the transfer of electrons from the incident to a diffracted beam.

The formation of the HOLZ lines is clearly represented in the sketch reported in Fig.2.2.6, where the bright (excess) HOLZ lines, due to the intersection of the Ewald sphere with the reciprocal lattice points of Miller indices (h_1,k_1,l_1), (h_2,k_2,l_2) and (h_3,k_3,l_3), are shown. The corresponding dark (deficit) HOLZ lines of these three reflections are evidenced in the central (transmitted) beam of this CBED pattern.

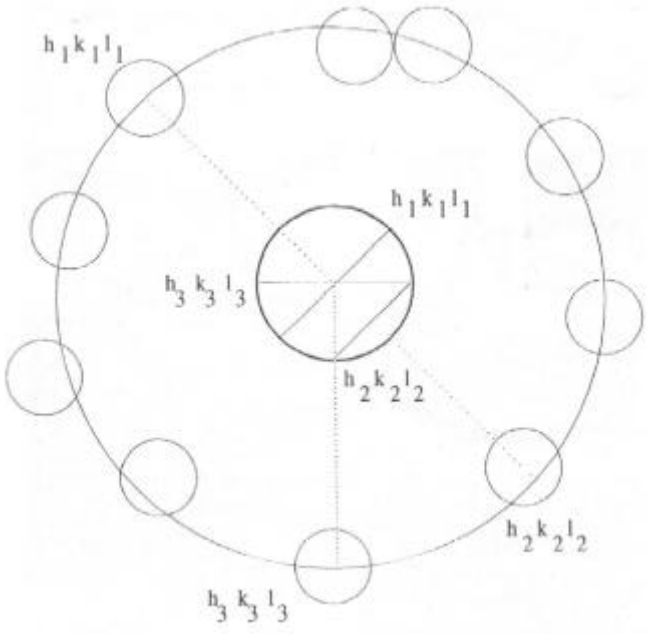

2.2.3

2.2.4

2.2.5 Figure 2.2.6

Sketch of a low magnification CBED pattern showing the FOLZ ring and diffracted disks, together with the transmitted central disk, which has been magnified for sake of clarity.
The three dark (deficit) lines in the central disk correspond to bright (excess) lines in the FOLZ.
The diffracted disks are not scaled with the FOLZ ring: in a real pattern the FOLZ lines inside each disk would appear are straight lines.

From this figure it is evident that in the central disk form all the lines corresponding to all the excess HOLZ lines. Their position depends on the lattice parameters of the crystal under

observation. This property has a fundamental consequence: variations in the lattice parameters can be detected through shifts in the HOLZ lines in the central disk. This explains why the TEM/CBED technique can be exploited to analyse strain tensors in crystals; moreover, this analysis can be performed on a nm scale. This is of paramount importance for the STREAM project, which aims at determining the strain distribution in deep sub-micron devices in a quantitative and automatic way.

2.3 Determination of the lattice parameters from the HOLZ line shifts

As mentioned in the previous section, the position of the HOLZ lines in the central (or (000)) disk in a CBED pattern depends on the geometry of the unit cell of the crystal under investigation in the TEM. It is therefore possible to deduce the local strain tensor from the analysis of the HOLZ line arrangement.

In Fig.2.2.7 are reported three CBED patterns obtained in silicon locally deformed in different ways. The nominal acceleration voltage of the TEM electrons is 100 kV and the cross-sectioned sample is tilted towards the <130> zone axis, which is 26.5° off the horizontal <110> orientation. The reason for the choice of this zone axis will be explained in the next section and depends on the availability of kinematically (rather than dynamically) diffracted HOLZ lines in the CBED pattern. The need for kinematic lines stems from the characteristics of the computer programme which simulates the CBED patterns, allowing one to obtain the strain tensor (see below).

The most intense HOLZ lines in the three patterns originate from the SOLZ, whereas the weaker (and finer) lines come from the fourth order Laue zone. It is worth noting that, when the sum of the <*uvw*> indices of the zone axis is even, as in the case of the <130> orientation (1+3+0=4) the odd-order Laue zones (e.g. FOLZ and third-order zone) are forbidden, due to the extinction of the corresponding diffracted beams.

It is evident the different shift of the HOLZ lines in the CBED patterns: the one on the left corresponds to a tensile deformation, namely the lattice parameter in the z direction is larger than in the undeformed silicon, which gives rise to the pattern in the centre of the figure. The pattern on the right originates from a compressive strain along the z direction of the silicon crystal.

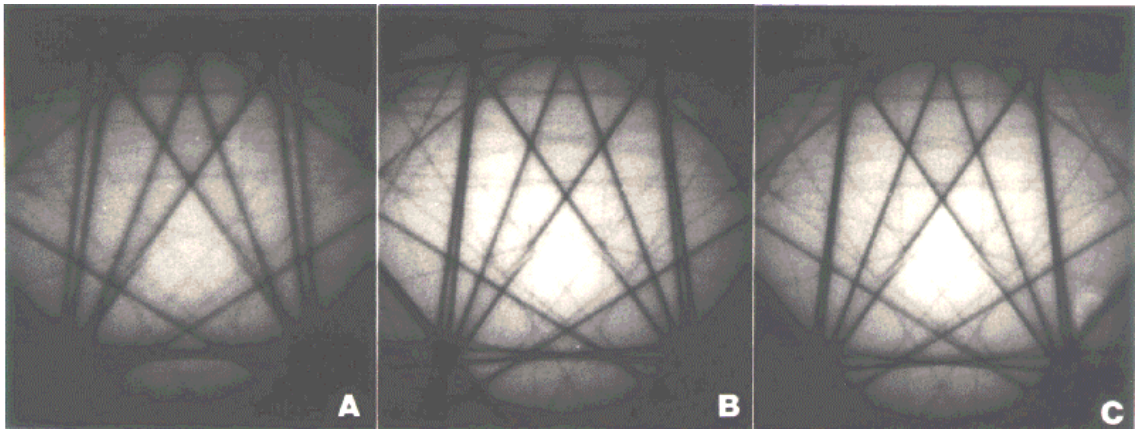

Figure 2.2.7
Central (transmitted) disks in the CBED patterns taken in three differently deformed positions in a crystalline silicon sample. A tensile strain along z is present in the region A, whereas in C this strain is compressive. The central pattern (B) is relative to undeformed silicon. The shift of the SOLZ lines is clearly visible. The weaker lines come from the fourth-order zone.
Acceleration voltage: 100 kV. Beam incident along a <130> direction.

In order to evaluate the effect of a strain on the position of the HOLZ lines, according to the kinematical approximation, assuming an isotropic deformation of a cubic crystal, one can start from the Bragg law in the small angle approximation (which holds for the electron energies typical of a TEM):

$$2d_{hkl}q = l$$

where d_{hkl} is the interplanar spacing of the set of $\{h\ k\ l\}$ planes and ϑ is the Bragg angle of the corresponding reflection. If the accelerating voltage (electron wavelength) is kept constant, differentiating the above equation with respect to a d_{hkl} and ϑ, one gets:

$$\frac{\Delta J}{J} = -\frac{\Delta a}{a} \qquad \left(d_{hkl} = \frac{a}{\sqrt{h^2 + k^2 + l^2}} \text{ in a cubic crystal like silicon}\right)$$

This means that a variation of the local lattice parameter (strain) results in a variation of the Bragg angle for the planes that give rise to a given HOLZ line and hence in a variation of its position.

However, if the differentiation is done with respect to λ and ϑ, keeping d_{hkl} constant (as in an undeformed silicon region), one finds that a variation in the TEM accelerating voltage ($\lambda \propto E^{-½}$) affects the position of the HOLZ line, as:

$$\frac{\Delta J}{J} = -\frac{\Delta E}{2E}$$

This evidences an ambiguity in the analysis of a CBED pattern: a given voltage variation can be misinterpreted as a strain, because both can induce a shift in the HOLZ line position. An example is given in the simulations in Fig.2.2.8. If the accelerating voltage is changed from 100 kV to 99 kV, the whole pattern of HOLZ lines is modified, as if some strain is present in the investigated area.

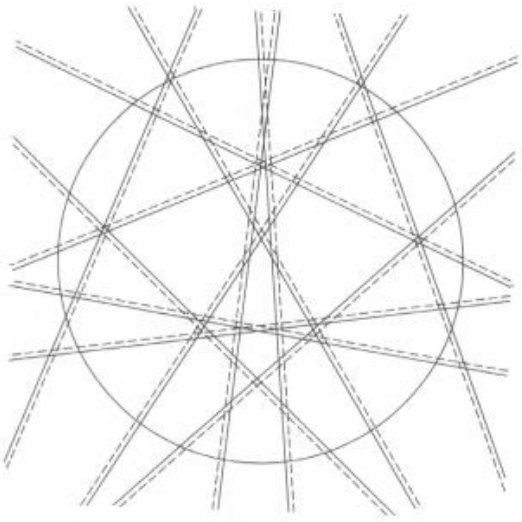

Figure 2.2.8

Effect of accelerating voltage on the HOLZ line position. CBED patterns simulated assuming a silicon crystal in a [-2 2 1] zone axis and a kinematical approximation. Solid lines: 100 kV; dashed lines: 99 kV

To solve this ambiguity, the usual procedure for strain analysis starts by taking a CBED pattern in a region of the sample which is surely undeformed. In a cross section of a device this is performed far from the active areas, i.e. in the silicon substrate. By comparing the experimental and the simulated patterns, the true (‘effective’) acceleration voltage is found. This value is assumed to

hold also in the strained region, what is correct only if the HOLZ lines chosen for the strain analysis are kinematical (see section 3).

It is now possible to evaluate the strain sensitivity of the CBED technique. It depends on the thickness of the sample in the analysed region. If the thickness is too small (<70 nm) the diffracted intensity markedly decreases and the HOLZ lines tend to vanish; conversely, if it is too large (>300 nm) the HOLZ lines become too broad. The experience gained at LAMEL on silicon suggests that a good compromise is a thickness of the order of 200 nm at 100 kV; in these conditions the electron energy loss due to plasmon excitation is about 40 eV. Consequently, if all the other factors are negligible, the maximum strain sensitivity of the CBED technique is:

$$\Delta a/a = \Delta E/(2E) \cong 40/(2*100.000) = 2*10^{-4}$$

Finally, two additional experimental conditions must be discussed:

- Choice of the acceleration voltage. The higher the voltage, the smaller the diffracted intensity; therefore the contrast of the HOLZ lines can become unacceptably low. For this reason a voltage of 100 kV is the most widely used one. During the STREAM activity, however, different voltages will be tested, particularly in the range 120-200 kV, which are typical of most modern microscopes (as the ones available in the ST and USFD laboratories). As HOLZ lines corresponding to different (*hkl*) planes will be generated, their kinematical or dynamical behaviour will be tested.

- Temperature of the specimen. Due to the fact that in a CBED pattern Laue zones higher than the the ZOLZ are excited, the HOLZ lines correspond to high index (*hkl*) planes. As such, their intensity is strongly affected by the thermal diffuse scattering, which is proportional to the summed squares of the Miller indices. Therefore the intensity of the lines will benefit from a decrease in the sample temperature: in fact, the CBED measurements were so far performed at a temperature of about 100 K, which is accomplished by using a LN_2 cooling holder. However, these holders limit the tilting capabilities of the goniometers available in some microscopes (particularly the ones with high resolution objective lenses, as in the case of USFD). For this reason, the STREAM project will also focus on this problem, exploring the feasibility of room temperature CBED experiments by using energy filtering of the electrons transmitted through the specimen. These filters are available in the TEMs installed in ST and in USFD.

3. Choice of the zone axis

From §2.2 it comes out that in a TEM, the HOLZ-line method is the most accurate one for lattice mismatch measurement between a substrate and overlying strained layers.

In a fully kinematical (i.e geometrical) approach the fitting procedure would start matching the HLP (HOLZ Line Pattern) taken in the substrate with the high voltage as the unique fitting parameter. Then assuming the transferability of the high voltage from the substrate to the strained layers, the unknown lattice parameters could be determined.

Unfortunately, this approach can be applied to the HLP simulation only if a limited accuracy is accepted[4], because it has been shown that, due to the crystal potential (projected along the zone axis direction) the HLP are rigorously modeled using dynamical formulation only[2].

However good accuracy (of the order of 10^{-4}) has been obtained using quasi-kinematical calculations which take into account the deviations from the pure geometric representation of the HLP produced by the crystal potential projected along the zone axis of incidence of electrons[5,6].

The quasi-kinematical approach is preferred because of its simplicity and computational speed, which is mandatory for mismatch evaluations through a best-fit procedure[6,7]. Briefly the following deviations must be carefully evaluated :

1. The accelerating voltage is generally underestimated at the center of the zone axis. This imply the use of an effective voltage in quasi-kinematical simulations of HOLZ patterns
2. The effective voltage depends on the projected potential then, in principle, it is different for different zone axes, incident directions of the convergent beam, materials and sample thickness

These dynamical effects can be rationalized if the role of the most important coefficient of the Fourier series of the projected potential of the sample (those associated to the zero layer diffracted beams) on the position of the HOLZ lines are taken into account. This is done through the study of the associated dispersion surfaces that give a picture of the allowed wave vectors (Bloch wave vector) for a given total beam energy and crystal potential. In fact, according to the general dynamical theory of diffraction the HOLZ line inside the central disk correspond to the intersection (hybridization) of the zero-layer dispersion surfaces with the ones corresponding to the High order Laue zone reflections (spherical surfaces due to the low value of their potential)[2].

Then a first order model for evaluation of the goodness of a zone axis is the three states Bloch wave model (two ZOLZ and one HOLZ)[8]. In this picture the HLP dependence from the projected potential is described by the ratio, R, between the excitation of the two ZOLZ branches. If R=const.>>1 for the different direction present in the cone of the convergent beam (the case of a very strong, flat ZOLZ branch hybridized with the HOLZ branch) the HOLZ line position is almost independent from the local projected potential of the sample and a unique effective voltage can be used in the quasi-kinematical simulations. For $R \approx 1$ a couplet of highly thickness-sensitive lines will be visible and finally when R<<1 it becomes difficult to record any deficiency HOLZ line.

According to this picture, the most important experimental parameter which must be accurately chosen in order to minimise the experimental errors is the zone axis. In fact the experimental errors in lattice parameters measurements by HOLZ line method are calculated from

$$s_a = \sqrt{s_d^2 + s_k^2 + a^2 \left[(s_{Eo}^2 + s_m^2) / (2 \times E_0)^2 \right]}$$

where σ_d is due to the error in the distance measurements from experimental HLP, σ_m is due to the the assumption of a flat dispersion surface, σ_k is due to the approximation of HOLZ lines by straight line, and σ_{Eo} is the error in the actual acceleration voltage measurement.

To select the best working conditions for lattice mismatch measurements through the HOLZ line method, we have compared plane sections of the dispersion surfaces of four commonly used zone axis in silicon: [111] ,[114], [001] and [130]. The plane sections of the dispersion surfaces have been drawn by solving the time independent Schroedinger equations in the Bloch waves formalism, using the bz1 routine of the EMS software package by Stadelmann[9], including 80 ZOLZ beams at 100 kV and varying the position of the center of the Laue circle along the reciprocal space direction, which corresponds to the strongest ZOLZ diffracted beam.
In Figure 3.1 are reported the results obtained for the four zone axes considered.

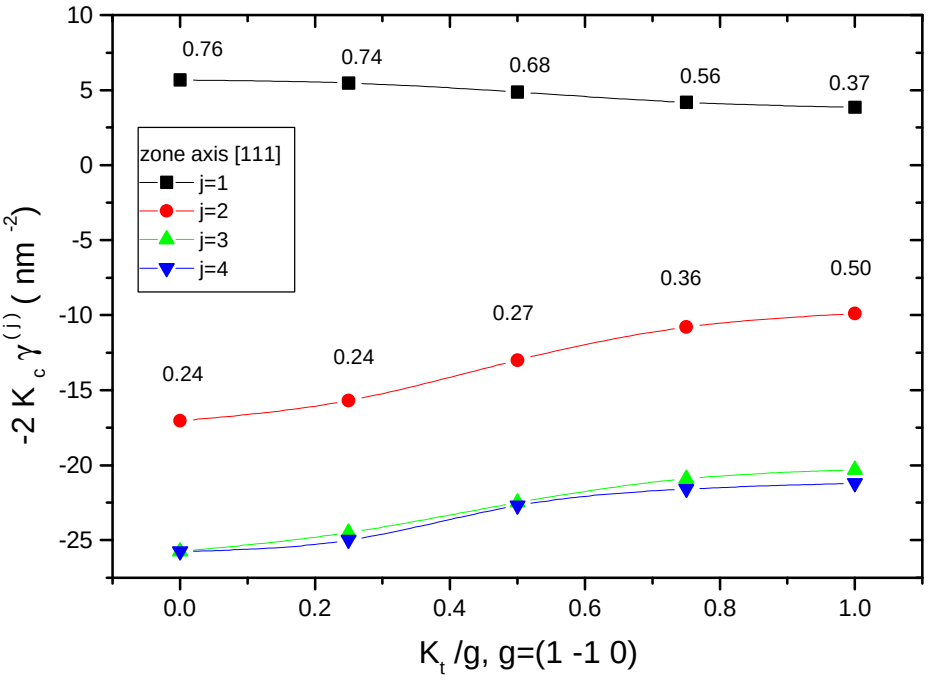

a)

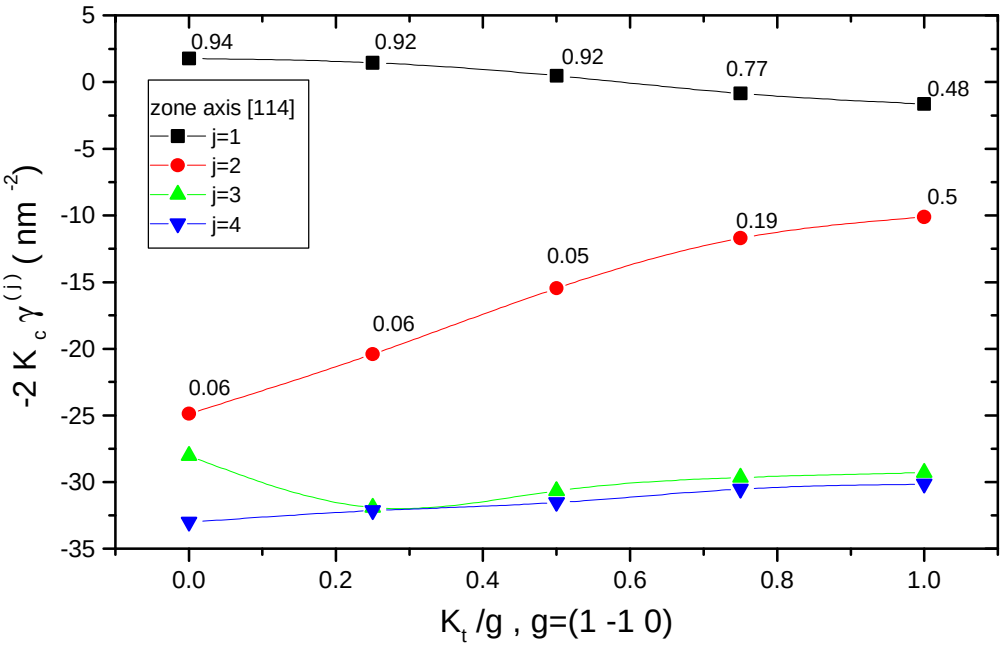
zone axis [114]
j=1
j=2
j=3
j=4
0.94
0.92
0.92
0.77
0.48
0.5
0.19
0.05
0.06
0.06
-2 K_c γ^(j) (nm^-2)
K_t /g , g=(1 -1 0)

b)

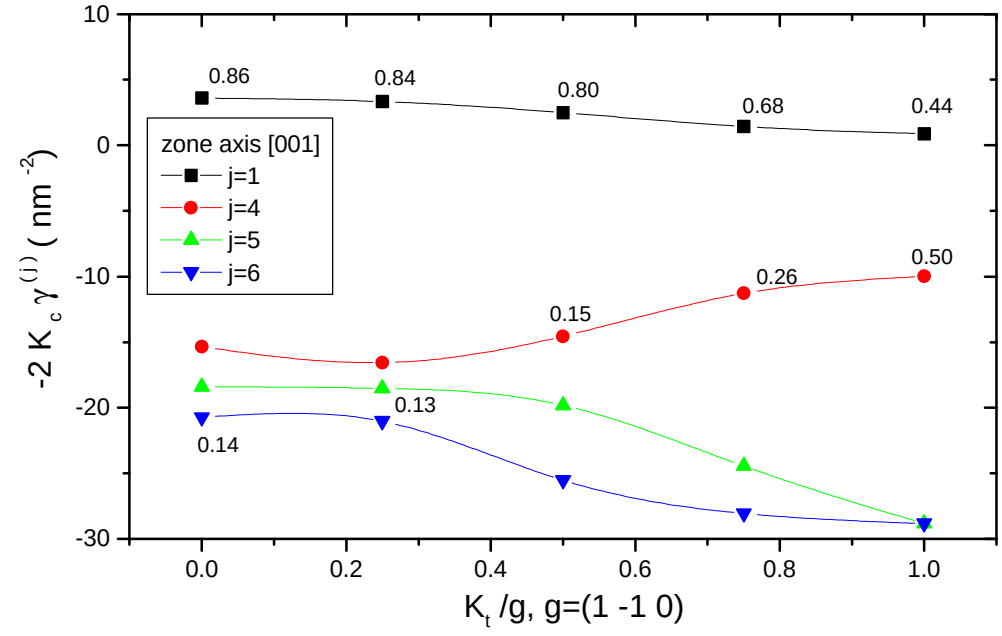
zone axis [001]
j=1
j=4
j=5
j=6
0.86
0.84
0.80
0.68
0.44
0.50
0.26
0.15
0.13
0.14
-2 K_c γ^(j) (nm^-2)
K_t /g, g=(1 -1 0)

c)

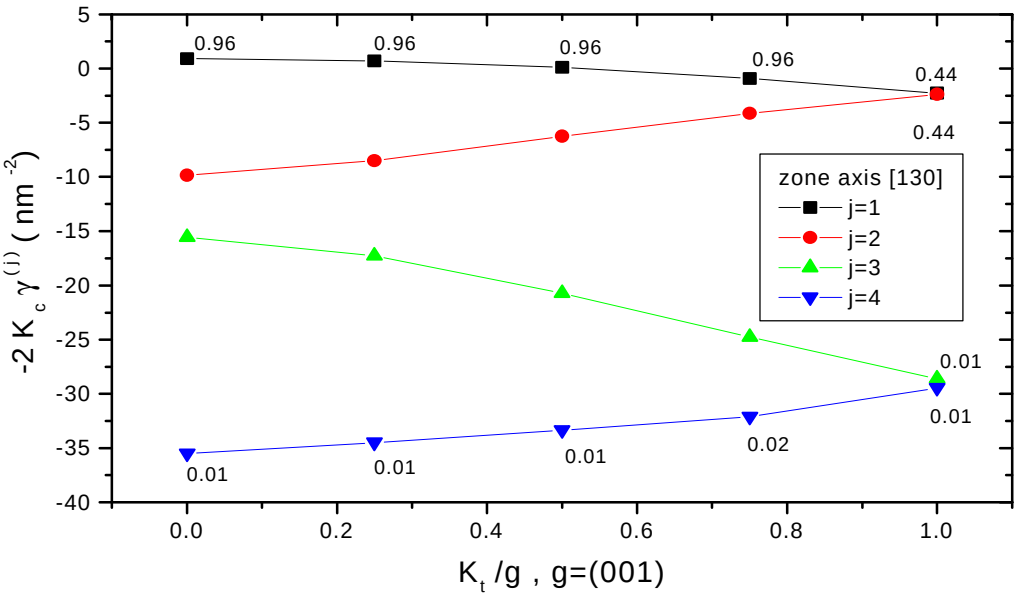

d)

Figure 3.1 Plot of a plane section of the dispersion surface of 100 kV elecrons impinging the specimen along the [111] a), [114] b), [001] c) and [130] d) zone axes in Silicon. $\mathbf{K_c}$ is the mean wave-vector inside the crystal; $\mathbf{K_t}$ is the tangential component of the incident wave vector; $\gamma^{(j)}$ is the eigenvalue of the Bloch states defined as $(\mathbf{K}^{(j)}-\mathbf{K_c})\ \mathbf{n}$. Here **n** is the outward normal of the TEM sample defining the positive z direction which is opposite to the electron wave vector. The excitations $|C^{(j)}_0|^2$ of the strongest Bloch states are also reported as small numbers superimposed to the plots. Absorption is neglected for the calculations.

It is evident that [130] zone axis is the best candidate for mismatch determinations, as it presents a dispersion surface with an almost flat first branch, highly excited and far enough from the second excited branch. In addition, through the dispersion surfaces it is possible to evaluate the correction ΔE to be applied to the actual high voltage in order to fit the experimental HLP with the kinematical calculations.

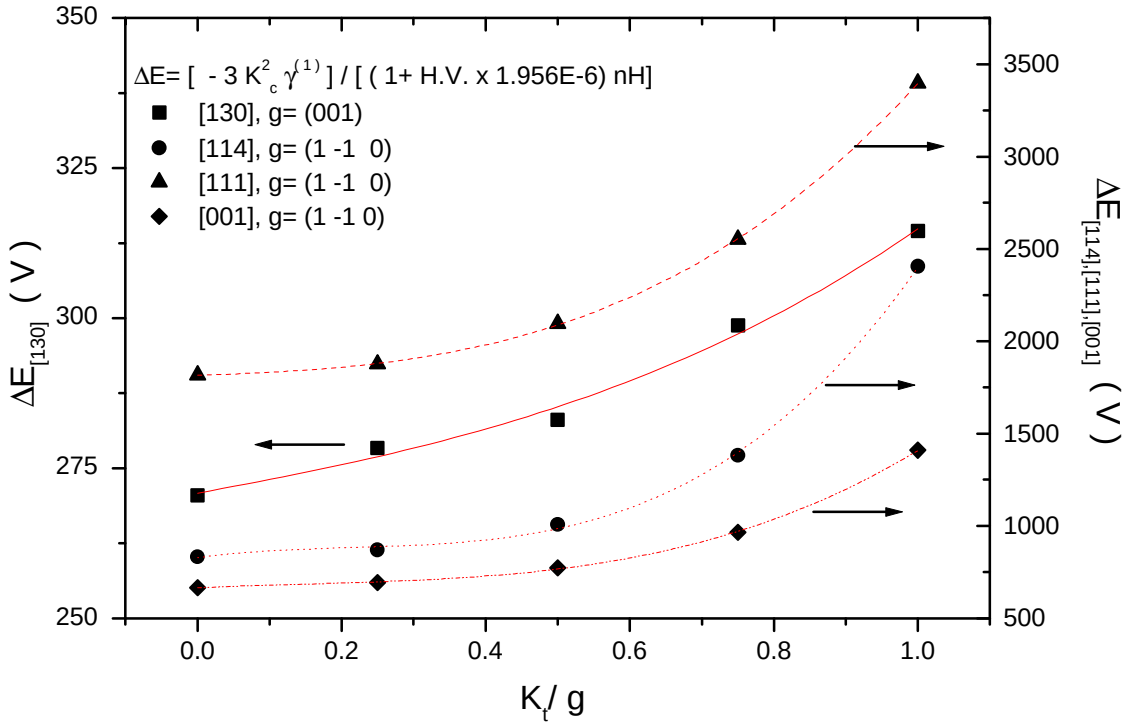

Figure 3.2 Plot of the correction factor ΔE to be applied to the high voltage for kinematical calculations as a function of the incidence angle of the electron as measured with respect to the zone axis. K_t /g =1 corresponds to the beam semicovergence as measured from the experimental patterns. H is the spacing between high order Laue zones numbered by (n).

Strictly, a different ΔE should be applied for different points of each HOLZ line in the pattern, however, as it can be seen in Figure 3.2, for [130] zone axis the variation in ΔE over the full range of semiconvergence is only 40 volts. This means that assuming a mean value <ΔE> = 290 volts results in an error σ_m = 20 volts, which as it will be shown below, is negligible with respect to the strain sensitivity of the technique. This is not the case of the [114], [001] and [111] zone axis, as for these orientations σ_m results equal to 350, 400 and 750 volts, respectively.

Finally, in order to check the independence of the HLP from the local thickness of the sample, we have applied the three Bloch states model to a typical HOLZ deficiency line visible in [130] zone axis. In Figure 3.3a is reported the intensity plot of rocking curves at 100 kV of the (1 -1 13) HOLZ line for different thickness of the sample. In the calculations it has been assumed *R*=96 which corresponds to the ratio of the excitations of ZOLZ dispersion branches as deduced from figure 2d. It is shown that in this case the position of the HOLZ deficiency line is almost independent from the thickness of the sample. For comparison, the calculations for line (5-711) observed in [111] zone axis at 122 kV (R=0.32) is also reported in Figure 3.3b. In this case a marked dependence

from the thickness is observed. For all the above considerations we have chosen the [130] orientation as the one which gives the most accurate results in strain determination at 100 kV.

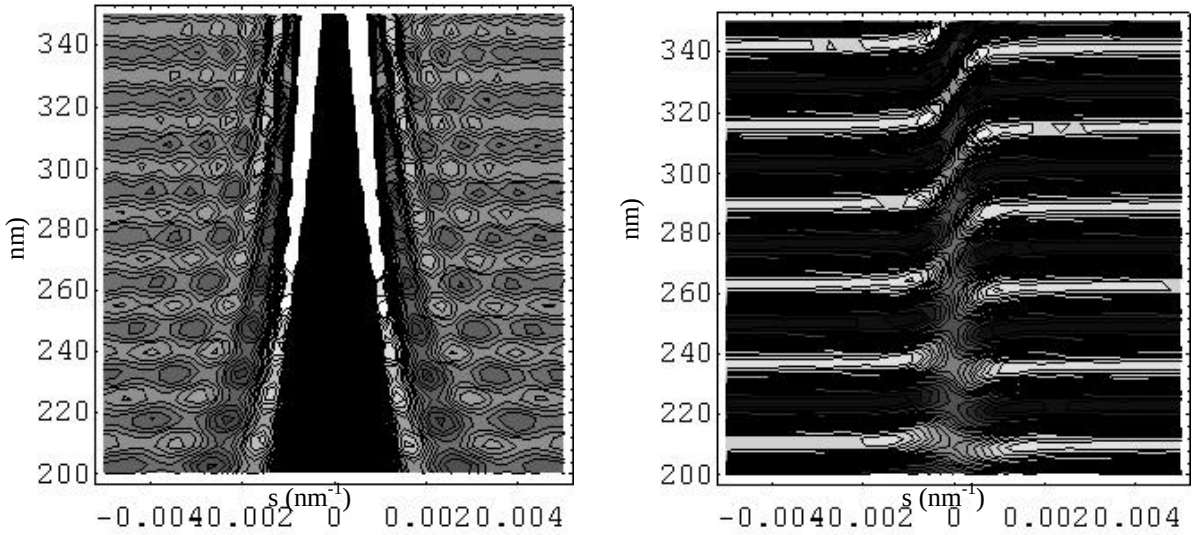

Figure 3.3 a) Contour plot of the rocking curve of the (1-1 13) HOLZ deficit line versus thickness of the sample. The curve is always symmetric with respect to the Bragg position of the line s=0. b)Contour plot of the rocking curve of the (5 -7 11) deficit line versus thickness of the sample.

4. Determination of the strain tensor

To determine the strain tensor values from the CBED patterns a semi-automatic procedure is adopted to compare the experimental patterns to computed ones.

After having chosen a suitable orientation (see Sect.3) the first problem to deal with is how to represent the experimental pattern in a numerical way. Since only quasi-kinematical theory of electron diffraction is used to simulate the patterns, they can be suitably represented by an array of lines (see Fig. 4.1) in place and in the same position of the original HOLZ lines. Two general methods have been reported in literature to parametrize such a skeleton. The area method consists in the measurement of the areas delimited by lines (see Fig. 4.2a), which will be compared with the corresponding ones from the theoretical patterns[10.] In the distance method instead, a set of distances is used, e.g. between the line crossing points (Fig. 4.2b)7. Both methods have some disadvantages: for example one can

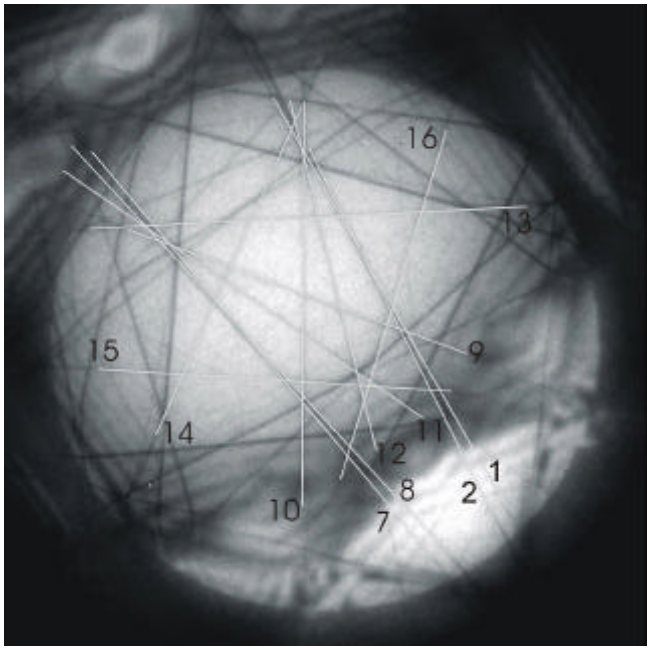

Figure 4.1 A [310] silicon CBED pattern taken at 100kV, with a skeleton of the HOLZ lines superimposed.

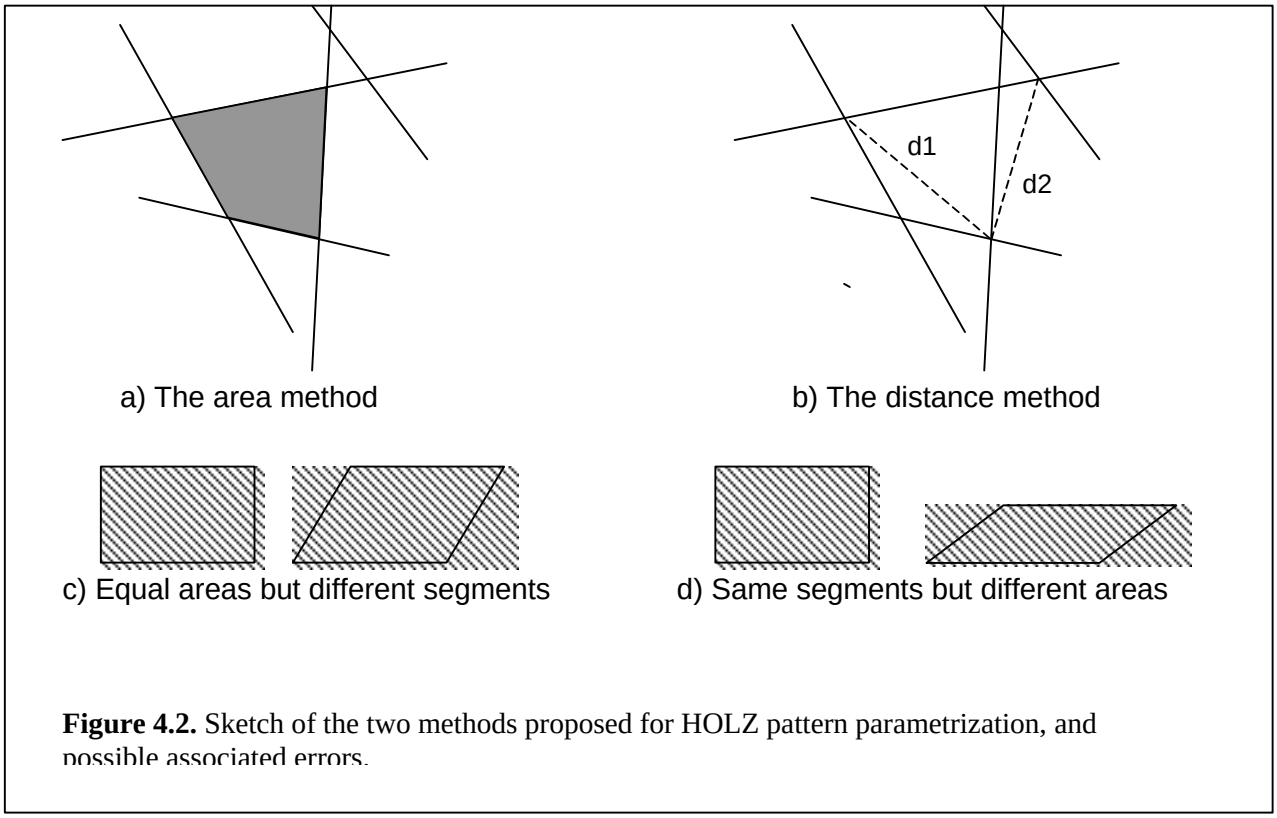

Figure 4.2. Sketch of the two methods proposed for HOLZ pattern parametrization, and possible associated errors.

think of two pictures with the same area but delimited by different segments and conversely it is possible to draw pictures with different areas delimited by the same segments (Fig. 4.2c,d). The

only way to reduce the errors is to increase the number of the measured elements, i.e. areas or distances, much more than the unknown to be determined (the six strain tensor components and the accelerating voltage).

We adopted so far the distance method, mainly because of its ease of use, since distances between crossing points can be easily measured also by hand, with a minimum error.

Then, the procedure adopted is as follows:

- The patterns are taken in the <130> silicon projection.
- A skeleton of the pattern is drawn, with up to 16 lines corresponding to HOLZ lines which, as it has been shown, can be simulated using the quasi-kinematical theory of electron diffraction.
- A (pre)defined set of distances is measured. An example of an input file for the program is shown on the right. The first column, ignored by the program, indicates the progressive number of the distance in the set. The second column is distance code out of the N(N-2)(N-1)/8 possible distances, where N is the total number of lines used. In the third and fourth columns are reported the measured distance and the error values, respectively.

input.txt

```
N.     LIST      "Any comment here"
1       1656      34.0     1.
2       1782      68.5     1.
3       1761      19.2     1.
4       1707      19.0     1.
5       1674      47.0     1.
6       1749      47.0     1.
7       1791      25.0     1.
8       1812      25.0     1.
9       1722      63.4     1.
10      1772      64.0     1.
11      1617      34.0     1.
12       699      34.0     1.
13      1637      61.3     1.
14       746      62.0     1.
15      1527      33.0     1.
16       396      32.7     1.
17      1551      61.2     1.
18       449      62.0     1.
19      1826      63.2     1.
20      1825      62.9     1.
21      1647      28.9     1.
22      1643      28.8     1.
23      1641      14.8     1.
24      1646      15.0     1.
25      1667      23.8     1.
26      1742      23.5     1.
27      1776      59.2     1.
28      1779      59.0     1.
29       655      40.0     1.
30       346      40.0     1.
31      1600      39.2     1.
32      1506      39.2     1.
33      1658      54.0     1.
34      1657      53.5     1.
35        12      26.5     2.
36         6      27.0     2.
37      1403      23.8     2.
38      1399      24.3     2.
39        57      50.8     2.
40      1421      48.8     2.
41        41      27.3     2.
42      1405      26.6     2.
43        50      35.0     2.
44      1414      37.0     2.
```

4.1 On the uniqueness of the strain tensor values as determined from CBED patterns

In principle, all the six components of the strain tensor can be deduced from a single CBED pattern. This is due to the sole feature of CBED patterns to include HOLZ lines, thus carrying full three-dimensional information of the reciprocal space. The components are obtained from the crystal lattice parameters, which are the minimisation routine output results, using the following formulae:

$$e_{ii} = \frac{a_i - a_{Si}}{a_{Si}} \qquad \text{with} \quad i=X,Y,Z$$

$$e_{YZ} = \frac{a - p/2}{2}, e_{XZ} = \frac{b - p/2}{2}, e_{XY} = \frac{g - p/2}{2}$$

where a_X, a_Y, a_Z, a, b and g are the unit cell parameters. In practice this result cannot be achieved in actual measurements because of the errors associated with HOLZ lines position determination, especially in case of small strain measurements: in most cases, there are many different combinations of the cell parameters giving rise to similar patterns.

This difficulty can be overcome in the investigation of electronic structures. These structures are presently grown on the silicon wafers along the <110> crystallographic directions, which is the same direction generally used for the specimen thinning for TEM sample preparation. As a consequence, in such samples, all the interfaces as well as the stress sources lie and act along these crystallographic directions. It can then be easily demonstrated (see fig.***) that the same distortion

Fig.4.1.1. Sketch of an isolation structure (LOCOS, see next Section) showing the two reference systems: the crystal axes system *XYZ* and the sample system *xyz.*

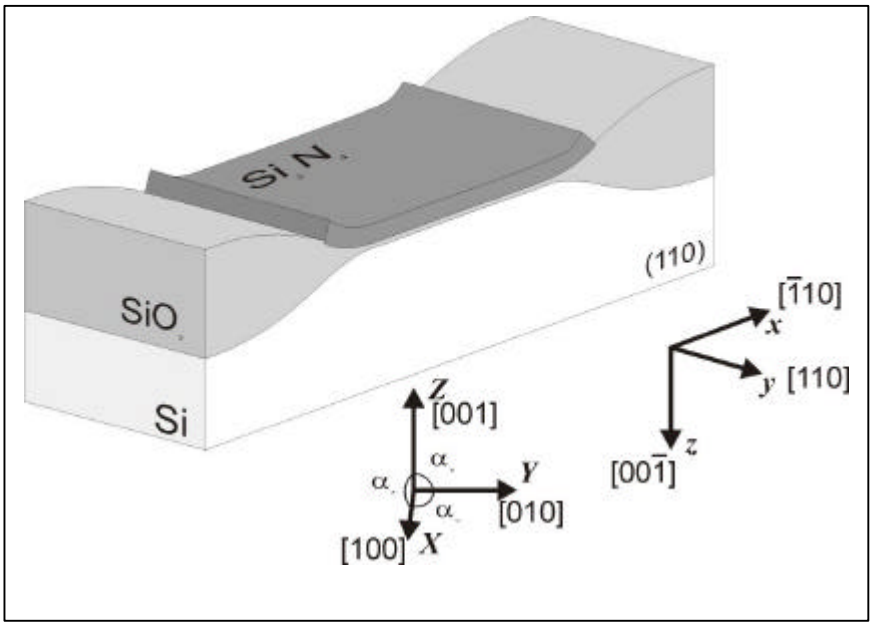

applies along the crystallographic directions X ([100]) and Y ([010]), since they both form angles of 45° with the [110] direction. An additional physical boundary is introduced after the specimen thinning for TEM analysis, but again this is a <110> direction, then every strain

relaxation along this direction, if any, generates the same distortion along the X and Y axes. Using the same arguments one can deduce that also the angles and β should be supplementary. The following conditions can then be written for electronic structures:

$$a_X = a_Y$$

$$a = -b$$

thus reducing from six to four the number of the unknown to be determined.

It is useful to define two reference systems in these samples. The first is the usual crystal system (XYZ in fig 4.1.1), the second is the so-called 'sample' system (xyz in fig 4.1.1), where the Z and z axes coincide while xy are rotated by 135 degrees about the Z axis from the XY axes position: the x and y axes are then <110> directions whereas all the other axes are <100>. It is important to point out that the crystal system only is used when performing quasi-kinematical simulations of the CBED patterns, i.e. the input and output cell parameters are defined in this system. The 'sample' system is mostly used to manage stress and strain in these sample (as said before, their sources are always oriented along <110> directions on the wafer plane); as an example, process simulator codes use this reference, in particular 2D simulators define quantities in a plane lying on the xz plane in fig.4.1.1. It is then important to define a set of equations which allow the transfer of quantities from one system to the other.

The question on how much stress can be relaxed with the specimen thinning for TEM observation deserves some attention. This amount is influenced by many factors. The most important is thickness, of course, but other components such as the absolute strain amount or its gradient should be taken into account. CBED strain measurements have also been performed in heterostructure deposited on Si substrates. In these structures this technique allows an exact determination of the specimen relaxation, due to the specimen thinning. It was found11 that, at thickness suitable for CBED analysis (not below 200 nm), the relaxation was at most 20%, leading to an error comparable (or even lower) to the error associated with the technique itself.

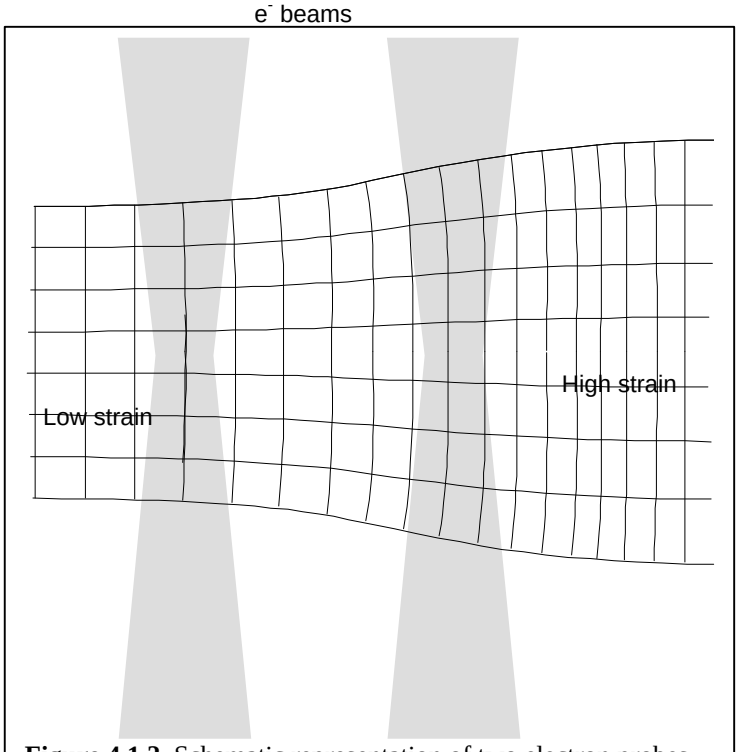

Figure 4.1.2. Schematic representation of two electron probes, sampling regions of different depth and lateral strain gradients.

Another important point is that stress relaxation, if any stress is present, is larger at the specimen surfaces if compared to the one occurring in the bulk. This is quite important when considering thinned specimen, since the relaxed volumes at the surfaces could be comparable with the bulk volumes. It must be pointed out that in CBED analysis, the information visible in the diffraction pattern comes from the whole analysed specimen volume: if the electron beam 'sees' a homogeneous crystal, a good pattern will result. On the other hand, if the beam analyses portions of the crystal with different deformation, the pattern should blur or even disappear. In fig.4.1.2 a section of TEM cross-section is shown with two electron beams crossing the sample. The

crystal lattice is represented by the thin crossing lines; the stress source is on the right, so that the strain values are expected to increase from left to right. Then the beam on the left will cross volumes with small strain values: also the horizontal strain gradient is expected to be small and the enhanced relaxation at the specimen surfaces involves small crystal portions if compared with the total analysed volume. A completely different situation is found on the right where larger strain values are present. Here there is a larger horizontal strain gradient and a strain variation is expected to occur as the beam proceeds through the specimen. In addition the combination of surface relaxation and strain gradient can generate shear strain components at the surface. In such situation the pattern quality rapidly degrades and eventually disappears.

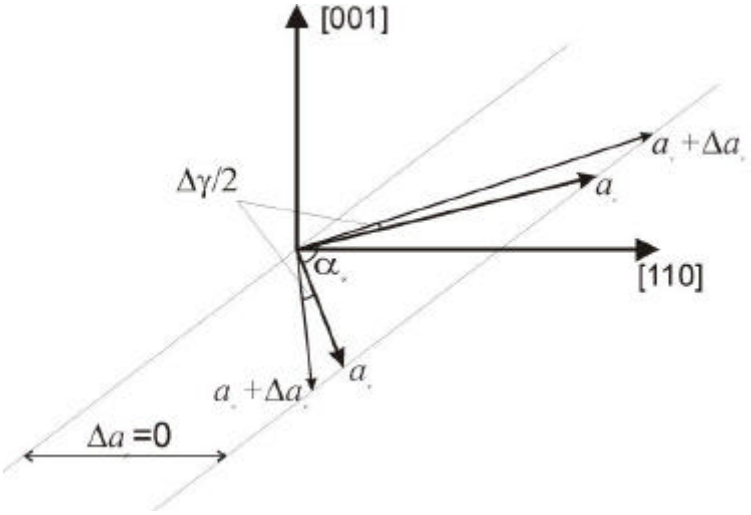

Figure 4.1.3. Correlation between ε_{XX} and $\Delta\gamma$, according to the plain strain approximation.

The above considerations lead to the conclusion the CBED cannot measure strain values too close to the stress source. On the other hand, once a CBED pattern has been successfully recorded, one can be confident that the strain was homogeneous in the analysed volume and the relaxation, even if present at the surfaces, is negligible if compared with the bulk strain values. It can then be concluded that, in device structures, if a good quality CBED pattern is obtained, then the strain relaxation can reasonably considered negligible. The maximum error associated with this assumption is at most of the same order with the errors associated with the technique itself.

This assumption, the so-called plane strain approximation, leads to a further reduction of the number of unknown to be determined. From fig. 4.1.3 it can be seen that by imposing that there is no stress relaxation along y (the thinning direction) the angle Z and the parameters aX=aY are mutually dependent and follow the relation

$$\frac{\Delta a_X}{a_X} = \frac{\Delta a_Y}{a_Y} = \frac{\Delta g / 2}{1 - \Delta g / 2} \approx \frac{\Delta g}{2}$$

This is particularly useful when measuring small strain fields, which is often the case in strain measurements performed in electronic devices. The small movement of HOLZ lines in the pattern does not allow to distinguish from many theoretical ones. However the introduction of the above constraint on the Z value always leads to a unique solution.

4.2 The HOLZFIT program structure

The minimization routine is made of one main program and six main subroutines.

In the main program, first all the program variables are initialized, then the input data are read.

The program can, in principle, work with any crystal in any orientation, provided the correct input data are given. Since the CBED technique has been applied so far to the <130> projection in silicon, all the input data which don't need to be redefined at each run (material, orientation, used reflections) have been collected in an include file (cfgini.inc).

`cfgini.inc`

```
*  This file contains the initialization values for all the variables which
*  doesn't need to be redefined at each minimization step.
*  If changed the program must be recompiled.


      data indz/3,1,0/                  ! zone axis
      data tilt/0.0,0.0,0.0/            ! centre of the Laue circle (3 real)
      data cl/8000.0/                   ! camera length


*  How many atoms are in the unit cell and how many species

      data natoms,ntype/8,1/


*  For each species write element name, atomic number and 9 gaussian
*  fitting parameters for atomic X-ray scattering factors

      label(1)='Si'
      zt(1)=14
      data (ax(j,1),bx(j,1),j=1,4),cx(1)/6.2915,2.4386,3.0353,32.370,
     *     1.9891,0.6758,1.5410,81.6937,1.1407/


*  For each site in the unit cell write atomic species number as previously
*  assigned, position (3 relative coordinates) and DW factor

      data (itype(i),i=1,8)/8*1/
      data (xp(j,1),j=1,3),dw(1)/0.0,0.0,0.0,0.46/
      data (xp(j,2),j=1,3),dw(2)/0.5,0.5,0.0,0.46/
      data (xp(j,3),j=1,3),dw(3)/0.5,0.0,0.5,0.46/
      data (xp(j,4),j=1,3),dw(4)/0.0,0.5,0.5,0.46/
      data (xp(j,5),j=1,3),dw(5)/0.25,0.25,0.25,0.46/
      data (xp(j,6),j=1,3),dw(6)/0.75,0.75,0.25,0.46/
      data (xp(j,7),j=1,3),dw(7)/0.75,0.25,0.75,0.46/
      data (xp(j,8),j=1,3),dw(8)/0.25,0.75,0.75,0.46/


*  Write the smallest two non-colinear g-vectors in the ZOLZ, and the
*  smallest from FOLZ

      data (gx(i),i=1,3)/0,0,1/(gy(i),i=1,3)/-1,3,0/
      data (gz(i),i=1,3)/0,1,0/


*  Order of the highest Laue zone + 1

      data iholz/3/



*  Nuber and indices of the beams

      data nbeams/16/
      data ((hkl(i,j),i=1,3),j=1,16)/1,-1,-13,
     *      0,2,14,5,-13,-1,5,-13,1,5,-13,3,5,-13,-3,
     *      1,-1,13,0,2,-14,3,-7,-11,3,-7,11,-1,5,-13,
     *      -1,5,13,-3,11,-7,-3,11,7,-3,11,-9,-3,11,9/

c23456789012345678901234567890c23456789012345678901234567890c23456789012345678901234567890c2345678901234567890
```

The file start.cfg contains all the variables which need redefinition at each run.

start.cfg

```
Choose the minimization task (0=voltage, 1=cell)
1
Effective voltage, step and range for variation (4 values)
```

```
99.29    0.01   99.00  100.00
Cell parameters, step and range for variation (4 values),equal flag
5.4288  0.01   5.4200 5.450   0
5.4288  0.01   5.4200 5.450   1
5.4288  0.01   5.4200 5.450   0
90.00   0.01    89.88 90.12     0
90.00   0.01    89.88 90.12     0
90.00   0.01    89.92 90.15     0
Limit for mag. determination
0.0001
Experimental data input file (two columns input)
input4.txt
Text output filename
pt41000d.out
Postcript output filename
out.ps
```

Since any CBED experiment first needs the determination of the effective accelerating voltage by simulating a pattern taken in the substrate, the first variable indicates which task is to be performed. Then, the voltage and the cell parameters are indicated: they will vary or remain fixed during simulation, depending on the chosen task. In each row the value variation step, the minimum and maximum values are also indicated. In the cell parameters rows there is an additional value: if zero, the corresponding parameter is treated as independent, otherwise it will be bound to other parameters.

The main program first calculates the electron wavelength and all matrices and vectors needed for crystal calculations. Second, as stated by the user on a separate files, only the actually measured distances are included in the distance list for the theoretical calculations. Then, the iterative procedure for the cell parameter (or the actual voltage) determination is started: at each iteration step the new cell parameters are calculated according to the input file start.cfg. The output data of each iteration consists of:

- The analytical parameters of the lines corresponding to the HOLZ lines
- The theoretical distance set
- The 2 value of the calculated set after comparison with the experimental one, after adjustment of the relative magnification
- At the end of the whole procedure the N best result (with the lower χ^2 value) are printed in the output file:

```
INCIDENT ELECTRON BEAM HIGH VOLTAGE    99.200000 KV
                        WAVELENGTH       .037177 A
                     CAMERA LENGTH  8000.000000 MM

                  NEAREST ZONE AXIS    3   1   0

THE INCIDENT BEAM DIRECTION : (     .000000     .000000     .000000 )

THERE ARE TOTAL   8 ATOMS AND  1 SPECIES

THE ATOMS, THEIR X-RAY SCATTERING FACTOR PARAMETERS
AND THEIR DEBYE-WALLER FACTOR

1  Si   Z= 14.00
 6.2915  2.4386  3.0353 32.3700  1.9891   .6758  1.5410 81.6937  1.1407

THE ATOMS TYPE, THEIR COORDINATES AND D-W FACTOR
1   .00000   .00000   .00000  .460 1   .50000   .50000   .00000  .460
1   .50000   .00000   .50000  .460 1   .00000   .50000   .50000  .460
1   .25000   .25000   .25000  .460 1   .75000   .75000   .25000  .460
1   .75000   .25000   .75000  .460 1   .25000   .75000   .75000  .460

BASE G VECTOR ALONG X DIRECTION    0   0   1
                    Y DIRECTION   -1   3   0
                    Z DIRECTION    0   1   0
```

```
TOTAL NUMBER OF BEAMS INCLUDED   16
   1  -1 -13,   0   2  14,   5 -13  -1,   5 -13   1,   5 -13   3
  5 -13  -3,   1  -1  13,   0   2 -14,   3  -7 -11,   3  -7  11
 -1   5 -13,  -1   5  13,  -3  11  -7,  -3  11   7,  -3  11  -9
 -3  11   9,

THE UNIT CELL IS DEFINED BY a =   5.42900 Angstrom
                            b =   5.42900 Angstrom
                            c =   5.42900 Angstrom
                        alpha =  90.00000 Degree
                         beta =  90.00000 Degree
                        gamma =  90.00000 Degree

Results
5.4320 5.4320 5.4300 90.02 90.02 89.98    .5228E-01    .9818
5.4340 5.4340 5.4310 90.02 90.02 89.98    .5519E-01    .9813
5.4320 5.4320 5.4300 90.03 90.03 89.98    .5644E-01    .9818
5.4300 5.4300 5.4290 90.02 90.02 89.98    .5780E-01    .9823
5.4340 5.4340 5.4310 90.03 90.03 89.98    .5987E-01    .9813
5.4300 5.4300 5.4290 90.03 90.03 89.98    .6147E-01    .9823
5.4280 5.4280 5.4280 90.02 90.02 89.98    .7180E-01    .9828
5.4280 5.4280 5.4280 90.03 90.03 89.98    .7497E-01    .9828
5.4320 5.4320 5.4300 90.01 90.01 89.98    .7832E-01    .9817
5.4340 5.4340 5.4310 90.01 90.01 89.98    .8065E-01    .9812
5.4300 5.4300 5.4290 90.01 90.01 89.98    .8441E-01    .9822
5.4320 5.4320 5.4300 90.04 90.04 89.98    .9073E-01    .9818
5.4340 5.4340 5.4310 90.04 90.04 89.98    .9459E-01    .9813
5.4300 5.4300 5.4290 90.04 90.04 89.98    .9532E-01    .9823
5.4280 5.4280 5.4280 90.01 90.01 89.98    .9898E-01    .9827
5.4280 5.4280 5.4280 90.04 90.04 89.98    .1084E+00    .9828
5.4330 5.4330 5.4310 90.02 90.02 89.96    .1270E+00    .9830
5.4310 5.4310 5.4300 90.02 90.02 89.96    .1296E+00    .9835
5.4320 5.4320 5.4300 90.00 90.00 89.98    .1346E+00    .9817
5.4340 5.4340 5.4310 90.00 90.00 89.98    .1363E+00    .9811
```

In the final part of the file the results are shown, ordered by increasing χ^2 value. The first six columns contain the cell parameters, then the χ^2 values and the magnification are reported.

5. Application to LOCOS structures

The TEM/CBED technique has been recently applied to determine the strain distribution along a cutline parallel to the padoxide/Si interface in a 0.80 μm wide recessed-LOCOS structure. The values of the components of the strain tensor so obtained have been compared with those computed by the simulator code IMPACT IV, which has been developed by the partner 3 of STREAM (ISEN, Lille). This 2D simulator can calculate the stress/strain distribution in devices such as LOCOS. The accuracy of the simulation is however critically dependent on the choice of the different physical parameters implemented into the code and some of them are still poorly known.

In order to make a suitable choice of the IMPACT IV parameters, the computed profiles of the components of the strain tensor are compared with the corresponding values obtained by CBED patterns taken in different points of TEM cross sections of the same structure. The programme HOLZFIT described in the previous section has been employed to obtain the experimental strain field distribution along the cutline.

5.1 Experimental details

A recessed LOCOS sample has been prepared for CBED analysis. The process flow for the sample preparation is the following[12]:

1) CZ Silicon substrate; 2) Stress relief oxide (10 nm) growth called *padoxide*; 3) Si_3N_4 film (117 nm) deposition by means of low pressure chemical vapour deposition (LPCVD) system (dichlorosilane and NH_3 based chemistry); 4) A lithographic step plus an etching step to define Si_3N_4 stripes (0.8 μm wide) and to reduce by 50 nm the level of silicon in the region not covered by nitride (recession); 5) Thick oxide growth (in our case 570 nm) called *field oxide*.

TEM <110> cross-sections of the LOCOS structures were analysed. They were prepared according to the procedure described in §2.2.

The specimens were investigated by using the Philips CM 30 TEM at the Istituto CNR-LAMEL. The accelerating voltage was 300 kV for imaging, and 100 kV for the CBED experiments. A Gatan liquid-nitrogen cooled double tilt holder was employed, in order to improve the HOLZ line visibility. The spot size at the specimen level was 10 nm, obtained in the nanoprobe mode.

5.2 TEM/CBED results

In Fig. 5.2.1a is reported a TEM micrograph of the LOCOS structure investigated in this work. From a morphological point of view it has to be noted the following features:

a) the lateral oxidation of silicon near the nitride edge called *bird's beak*; b) the growth of the pad oxide thickness during the field oxidation called *padoxide punch through*; c) the abrupt oxide/silicon interface discontinuity near the edge of silicon nitride; d) the reduction of the final field oxide thickness in narrow space called *field oxide thinning*.

The values of the different geometrical parameters are shown in Table I and compared with the expected ones. The values of the parameters are generally in mutual good agreement, except for the pad oxide thickness which results to be 52 nm instead of the expected 11 nm and for the field oxide thickness (474 nm instead of 570 nm). This is due to the well known *bird's beak punch through* and *field oxide thinning* phenomena. This discrepancy will strongly affect the simulation of the technological process, as it will be discussed in the next paragraph.

Table 4 Geometrical parameters of the LOCOS structure. The agreement between the designed and the real values is generally good, except for the thickness of the *pad* and *field oxides*.

	Pitch (mm)	Nitride width (mm)	Nitride thick. (nm)	Pad oxide thick. (nm)	Field oxide thick. (nm)
Design	1.3	0.80	117	10	570
TEM	1.36	0.80	110	52	474

On the structure reported in Fig.5.2.1a, CBED patterns have been taken in nine points located along a cut line, at a depth of 200 nm from the pad/substrate interface, as sketched in Fig.5.2.1b. It must be noted that the strain values, as measured by CBED, are given in the cubic unit cell system (indices in caps), where the X,Y and Z axes are directed along the [100], the [010] and the [001] crystallographic directions, respectively. Instead, as it will be seen in the next section, the process simulation codes assume a 'sample-based' frame of reference (x,y,z), where z≡Z=[001], x and y are orthogonal <110> directions in the wafer plane (y being parallel to the length of the nitride stripe) (see §4.1).

From the comparison between the experimental CBED patterns and the simulated ones, the different components of the strain tensor in the nine selected points have been determined. In Fig.5.2.2 the plots of the ε_{XX}, ε_{ZZ} and ε_{XZ} are reported.

5.3 Process simulation of the LOCOS structure

In this section the results of the morphological simulations of the structure above described and the subsequent calculation of the stress and strain field inside the silicon substrate are reported. The morphological simulations of the structure have been performed using the same set of coefficients calibrated during a previous work. The implementation of the model of stress relief produces an effect also on the morphological profile of the simulated structure; most of the differences are related to the thickness of the oxide grown under the silicon nitride (*padoxide*). Depending on the model, the computed *padoxide* thickness either retains its initial value (around 10 nm), or it grows until it reaches the value of 50 nm, much closer to the measured one (Fig.5.3.1). This effect may be ascribed directly to the different stress relief models and in particular to the calculation of the reaction rate at the silicon-oxide interface which is reduced by the stress normal to the interface (Kao, 1988)***. When it is allowed to relax the stress in the silicon (Fig. 5.3.1), the value normal to the interface will never reach values able to effectively reduce the reaction rate, then the oxide is grown freely at the interface. On the other hand, if the model of stress relief is not activated the value accumulated during the oxidation time will be able to inhibit the reaction rate, then a thinner oxide thickness is expected in this case.

Unlike the commercial simulator ATHENA (based on the well known SUPREM code, developed at the Stanford University), where the stress field inside the silicon substrate is calculated only at the end of the oxidation step, IMPACT performs this computation during the growth of the field oxide. The set of equations implemented consists of an equilibrium relationship calculated for the bulk substrate and a boundary condition applied to each node of the silicon oxide interface proportional to the velocity of the interface inside the substrate:

$$\frac{\partial \sigma_{xx}}{\partial x} + \frac{\partial \sigma_{xz}}{\partial z} = 0$$

$$\frac{\partial \sigma_{zz}}{\partial z} + \frac{\partial \sigma_{zx}}{\partial x} = 0$$

To convert the stress values into strain data for comparison with the CBED results, the following equations have been applied:

$$e_{XX} = e_{YY} = 2.77 \cdot 10^{-12} s_{xx} - 2.14 \cdot 10^{-12} s_{zz}$$
$$e_{ZZ} = -2.14 \cdot 10^{-12} s_{xx} + 7.68 \cdot 10^{-12} s_{zz}$$
$$e_{XY} = \Delta g / 2 = 3.175 \cdot 10^{-12} s_{xx};$$
$$e_{YZ} = -e_{XZ} = \Delta a / 2 = -\Delta b / 2 = 4.49 \cdot 10^{-12} s_{xz}$$

The simulations obtained with IMPACT showed a qualitatively correct behaviour of the strain, but at the same time an overestimation of the same quantities. Moreover, the simulation show significant morphological differences with respect to the real sample, particularly for the *bird's beak punch through* phenomenon. As a consequence it has been tried to modify the internal code of IMPACT in order to neglect the accumulation of the stress during the simulation of the oxide growth.

The results of the simulation so obtained are reported in fig.5.3.1: it can be observed the good agreement of the experimental points and the simulated ones. Furthermore it is maintained the symmetric contour along the whole cross section. Also the *bird's beak punch through* phenomenon is accurately replicated (see fig 5.3.1). It is important to observe that the encouraging results obtained with this modification does not allow to generalise the assumption of full stress relaxation. In our opinion it can only be stated that for this particular process condition (oxidation temperature: 1000 C for about 135 min) the stress relaxation occurs during the oxidation time, so that it can be modelled without taking into account the whole accumulation.

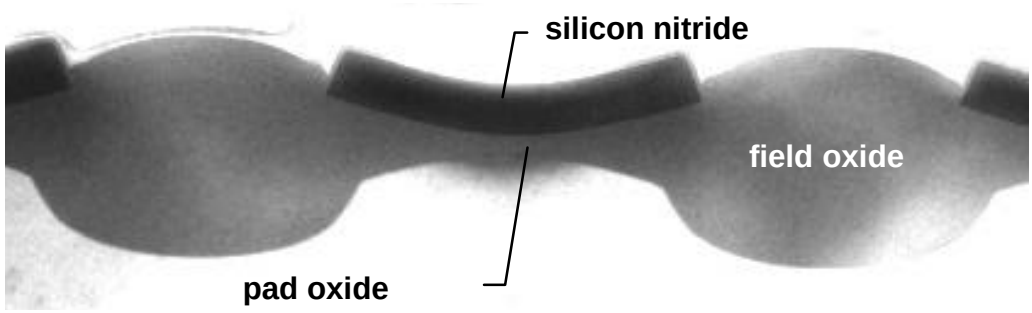

a

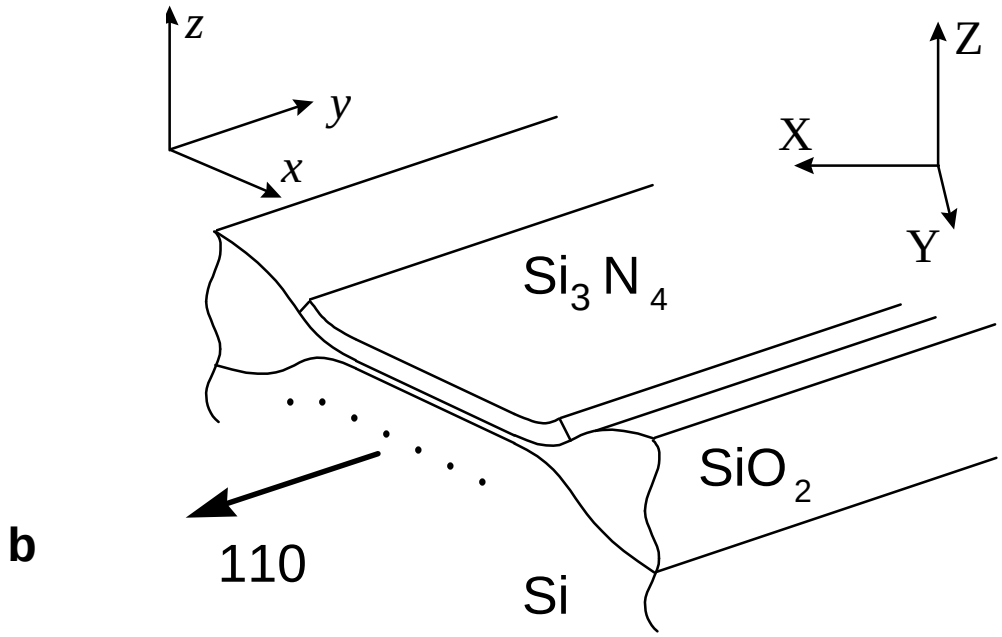

Figure 5.2.1. a). Bright field TEM micrograph of the LOCOS structure. b) TEM image of the investigated LOCOS structure, showing how a series of CBED pattern can be obtained by focusing the electron beam onto a 10 nm spot along a cutline. The "sample-based" (*x*,*y*,*z*) and the unit cell (X,Y,Z) reference systems are also shown.

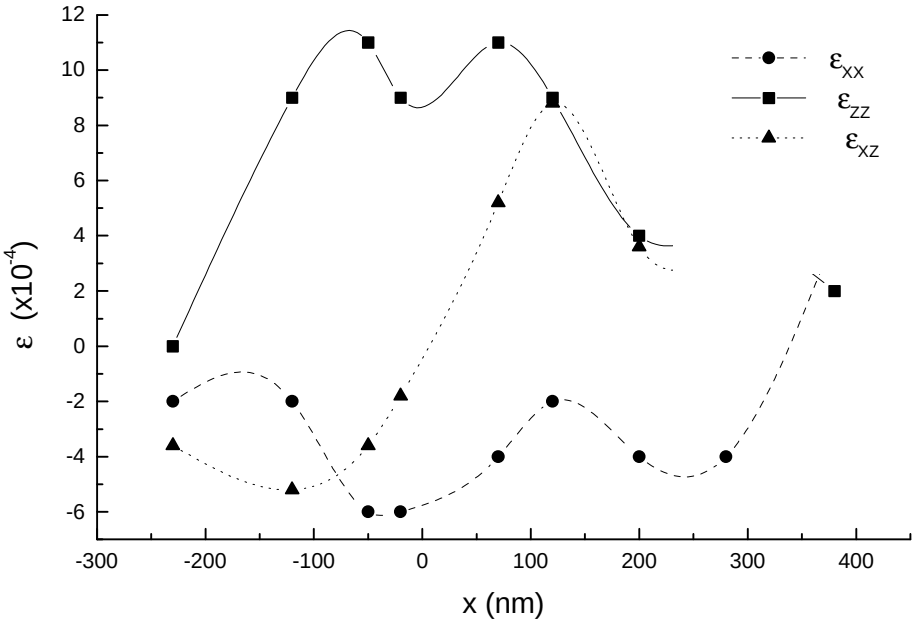

Figure 5.2.2. Components of the strain tensor, as deduced from the CBED measurements, taken in the points sketched in Fig.5.2.1b. The *x* abscissa is parallel to the cutline. The curves are drawn only to guide the eyes.

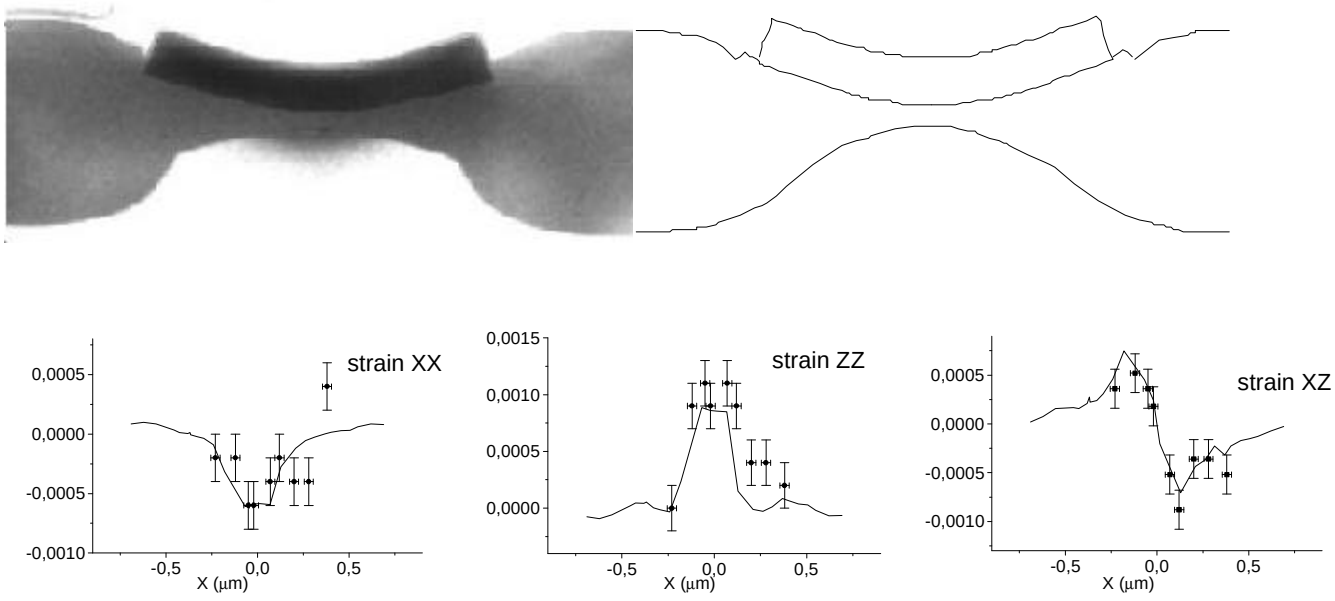

Figure 5.3.1 (top) Cross-sectional TEM image and corresponding simulated (IMPACT) morphology of the 0.80 μm LOCOS structure; (bottom) Comparison between TEM/CBED (points with error bars) and simulated (continuous line) values of strain components along a cutline at z=200 nm below the padoxide/substrate interface.

6. Conclusions

In this work it has been demonstrated that the TEM/CBED technique can be successfully applied to the determination of the strain distribution, as well as of the morphology of a sub-micron LOCOS isolation structure. These results have been compared with ones deduced from a two dimensional process simulator (IMPACT), developed by partner 3 of STREAM (ISEN, Lille).

During the project activity, these TEM/CBED analyses will be applied to the state-of-the-art shallow trench isolation (STI) structures, which have nowadays replaced the LOCOS, due to its intolerably large dimensions of the oxide bird's beak, which makes it unusable for critical dimensions of 0.25 μm and below. These STI will be implemented into the STREAM test structures for the 0.15 μm generation of non volatile memories.

References

[1] D.B.Williams and C.B.Carter, *Transmission Electron Microscopy*, Vol.2 Plenum Press New York, 1996)

[2] P.M.Jones, G.M.Rackham and J.W.Steeds, Proc.Roy.Soc. A354 (1977) 197

[3] J.W.Steeds and E.Carlino, in: *Electron Microscopy in Materials Science*, ed. by P.G.Merli and M.Vittori Antisari (World Scientific, Singapore, 1992) p.279

[4] E.G.Bithell and W.M.Stobbs, J.Microsc. 153 (1989) 39

[5] D.M.Maher, H.L.Fraser, C.J.Humphreys, R.W.Knoell and J.C.Bean, Appl.Phys.Lett. 50 (1987) 574

[6] R.Balboni, S.Frabboni and A.Armigliato, Phil.Mag. A77 (1998) 67

[7] J.M.Zuo, Ultramicroscopy 41 (1992) 211

[8] J.Mansfield, D.Bird and M.Saunders, Ultramicrosocpy 48 (1993) 1

[9] P.Stadelmann, Ultramicroscopy 21 (1987) 131

[10] S.J.Rozeveld and J.M.Howe, Ultramicroscopy 50 (1993) 41

[11] J.Vanhellemont, K.G.F.Janssens, S.Frabboni, P.Smeys, R.Balboni and A.Armigliato, MRS Symposium Proc. Vol. 405 ed. by S.M.Prokes, R.C.Cammarata, K.L.Wong and A.Christou (Pittsburgh, PA, 1995) p.435

[12] A.Armigliato, R.Balboni, S.Balboni, S.Frabboni, A.Tixier, G.P.Carnevale, P.Colpani, G.Pavia and A.Marmiroli, Micron 31 (2000) 203